Reversible transformation between bipolar memory switching and bidirectional threshold switching in 2D layered K-birnessite nanosheets

Meilin Tu[1⊥], Haipeng Lu[2⊥], Songwen Luo[1], Hao Peng[3], Shangdong Li[3], Yizhen Ke[3], Shuoguo Yuan[4], Wen Huang[3], Wenjing Jie[1], Jianhua Hao[4]**

[1]College of Chemistry and Materials Science, Sichuan Normal University, Chengdu, 610066, China

2 National Engineering Research Center of Electromagnetic Radiation Control Materials, University of Electronic Science and Technology of China, Chengdu,610054

3 State Key Laboratory of Electronic Thin Films and Integrated Devices, School of electronic Science and Engineering, University of Electronic Science and Technology of China, Chengdu, 610054, China.

4 Department of Applied Physics, The Hong Kong Polytechnic University, Hung Hom, Kowloon, Hong Kong, China.

KEYWORDS: 2D layered nanosheets; K-birnessite; resistive switching; memory switching; threshold switching

ABSTRACT

Birnessite-related manganese dioxides (MnO_2) have recently been studied owing to their diverse low-dimensional layered structures and potential applications in energy devices. The birnessite MnO_2 possesses a layered structure with edge-shared MnO_6 octahedra layer stacked with interlayer of cations. The unique layered structure may provide some distinct electrical properties for the 2D layered nanosheets. In this work, layered K-birnessite MnO_2 samples are synthesized by a hydrothermal method. The resistive switching (RS) devices based on single K-birnessite MnO_2 nanosheets are fabricated by transferring the nanosheets onto SiO_2/Si substrates through a facile and feasible method of mechanical exfoliation. The device exhibits nonvolatile memory switching (MS) behaviors with high current ON/OFF ratio of ~ 2×10^5. And more importantly, reversible transformation between the nonvolatile MS and volatile threshold switching (TS) can be achieved in the single layered nanosheet through tuning the magnitude of compliance current (I_{cc}). To be more specific, a relatively high I_{cc} (1 mA) can trigger the non-volatile MS behaviors, while a relatively low I_{cc} (≤ 100 μA) can generate volatile TS characteristics. This work not only demonstrates the memristor based on single birnessite-related MnO_2 nanosheet, but also offers an insight into understanding the complex resistive switching types and relevant physical mechanisms of the 2D layered oxide nanosheets.

INTRODUCTION

Nanoscale materials may exhibit promising properties that are rarely present in their bulk counterparts.[1] A wide variety of nanomaterials have been synthesized and studied extensively in this century, from zero-dimensional (0D) nanoparticles and/or quantum dots, one-dimensional (1D) nanotubes and/or nanowires to two-dimensional (2D) layered nanosheets.[2,3] Among them, 2D layered materials have drawn much attention ever since the discovery of graphene and extensively studied compounds of transition metal dichalogenides (TMDCs).[4,5] Beyond graphene and TMDCs, a series of 2D materials have been exfoliated from their bulk crystals and fabricated through physical and chemical methods.[6,7] Manganese dioxide (MnO_2) is an important functional oxide owing to its structural diversity, amazing physical and chemical properties as well as wide-range applications in energy, catalysts, and biomedicines.[8,9] Among them, birnessite-related manganese dioxide with A_xMnO_2 structure where A stands for H^+ or metal cation is emerged.[10] The birnessite manganese dioxide has a layered structure that consists of edge-shared MnO_6 octahedra layer with cations and water molecules occupying the interlayer region.[11,12] Such birnessite-typed manganese dioxides with 1D and 2D forms have been synthesized and characterized, aiming at their potential applications in rechargeable battery.[13,14] Recently, 1D MnO_x nanorods showed memristive properties under moisture ambient, while the memristive behaviors vanished under dry ambient.[15] Actually, some 1D and 2D materials have been widely used in recently developed memristive devices[16,17] Generally, a memristor is a two-terminal resistive switching (RS) device with sandwiched structure and its resistance states depend on the external bias voltage. The memristor has received considerable attention towards promising non-volatile memory, logic device and computing applications. Memristors have been fabricated using a diverse range of 2D materials, from graphene,[18,19] graphene oxide,[20] TMDCs,[21–24] III-VI

GaSe,[25] hexagonal boron nitride[17] to black phosphorous.[26] In comparison with traditional thin film based RS devices, memristors based on the 2D layered nanosheets not only provide atomically thin platform for memory but also show relatively lower operating voltages, suggesting promising applications in energy-efficient memristor-based neural networks.[22,27] Until now, 2D layered birnessite MnO_2 has been widely studied in energy devices of batteries and capacitors.[9,28] However, there is no exploration on the memristors using the recently-developed 2D layered birnessite manganese dioxide. By considering the unique 2D layered structure, it is expected that such birnessite MnO_2 nanosheets could demonstrate some intriguing resistive switching properties. In this work, layered K-birnessite MnO_2 samples were synthesized by a hydrothermal method. The RS devices based on single K-birnessite MnO_2 nanosheets were fabricated by transferring the nanosheets onto SiO_2/Si substrates through mechanical exfoliation method. By considering it is difficult to achieve the 2D layered MnO_2 nanosheets through bottom-up techniques, our exfoliation method is a facile and feasible way to fabricate conceptual device. Here, Ag electrodes were prepared through photolithography technique to form lateral device. The nonvolatile memory switching (MS) behaviors can be observed in single K-birnessite MnO_2 nanosheet. Importantly, controllable transformation between the nonvolatile MS and volatile threshold switching (TS) can be achieved in such layered nanosheet through tuning external stimulations of compliance current (I_{cc}). This work would help one to study the complex RS types and understand the underlying physical mechanism based on the unique 2D layered oxide nanosheets.

EXPERIMENTAL SECTION

Material Synthesis: The K-birnessite MnO_2 nanosheets were synthesized by hydrothermal method. 1 mmol potassium permanganate was mixed well with 28 mL deionized water. Then,

0.6 mol potassium hydroxide was quickly added to the mixed solution and then the solution was stirred vigorously. After that, 2 mL manganese sulfate (1 mol/L) was added in the mixed solution. Since the addition of a large amount of potassium hydroxide could generate a large amount of heat during the dissolution process, the mixed solution was stirred for 2 h after all the materials were added. The cooled solution was poured in a 50 mL Teflon-lined autoclave which was sealed and placed in an oven for 175 °C for 48 h. Then, the autoclave was naturally cooled down to room temperature. The black reaction products were washed with distilled water and ethanol, and then stored in distilled water.

Device fabrication: 2D layered K-birnessite MnO_2 nanosheets were prepared and transferred onto SiO_2/Si substrate using micromechanical exfoliation by scotch-tape method. Firstly, a small piece of the prepared MnO_2 sample was put on a scotch tape. The tape was refolded, pressed and then unfolded, in order to achieve 2D layered MnO_2 nanosheets. Then, the nanosheets were transferred from the tape onto SiO_2 substrate. Subsequently, 2D layered MnO_2 nanosheets with the size from a few to dozens of micrometres can be achieved. Then, the electrode pattern was prepared by photolithography on the individual nanosheet. And Ag electrodes with the thickness of ~ 100 nm were prepared by using sputtering method. Then the photoresist and excess Ag were ultrasonically cleaned with acetone. Finally, the fabricated devices were dried at 100 °C.

Characterizations and measurements: The crystal structure of the prepared samples was characterized by the X-ray diffraction (XRD) technique with Cu Kα (λ= 1.540598 Å) radiation (Smart Lab, Riga ku) in the 2 θ range of 10° ~ 80°. The microstructure of the samples was investigated by field emission scanning electron microscope (FESEM, JSM-7800F, Japan) and transmission electron microscope (TEM, JEM-2100, Japan). The surface morphology and thickness of the exfoliated K-birnessite MnO_2 nanosheets were characterized by atomic force

microscopy (AFM, DI Nanocope 8). Raman microscope (532 nm, Witec Confocal Raman Microscope alpha 300 R) was used to perform Raman and photoluminescence (PL) characterizations. The X-ray photoelectron spectroscope (XPS) (Thermo Scientific ESCALAB 250Xi) was used for determining chemical environment and elemental analysis. All the RS measurements were performed by double channel Keithley 2636B SourceMeter with a four-probe station system. All measurements were carried out in air at room temperature.

RESULTS AND DISCUSSION

The K-birnessite MnO_2 possesses layered structure (Figure 1a) with the edge-shared octahedra layer vertically stacked with adjacent layer of some K cations (K^+) and water molecules. The Mn-O octahedron is formed by manganese at the center and oxygen at each vertex of the octahedron (inset of Figure 1a).[29,30] In our experiments, the K-birnessite MnO_2 samples were synthesized by hydrothermal method through adding potassium hydroxide solution. The interlayer cations and water molecules maintain the layered structure of the MnO_2, owing to the presence of interlayer electrostatic attraction and/or van der Waals forces.[11,30,31] Figure 1b shows the FESEM image of the synthesized K-birnessite MnO_2, indicating the nanosheet structure of the synthesized materials. Furthermore, XRD technique has been employed to characterize the crystal structure of K-birnessite MnO_2, as shown in Figure 1c. Two sharp (001) and (002) peaks, located at ~ 12.5 ° and 25.2 °, respectively, indicate excellent crystallinity and prove the existence of layered structure of the prepared materials. The standard card shows that the space group of the crystal is C / 2m, and its lattice constants are a = 5.1490 Å, b = 2.8430 Å, c = 7.1760 Å, and β = 100.7600 °.[32] The interplanar spacing of the crystal plane of (001) is about 7 Å that corresponds to the lattice constant c = 7.1760 Å. There is a weak impurity peak located at ~ 17.5°, which can be found to match well with the standard card PDF # 80-0328 of Mn_3O_4 [33].

During the synthesis process, a large amount of heat can be generated when potassium hydroxide is rapidly added into water, which could cause some manganese hydroxide ($Mn(OH)_2$) to be oxidized into Mn_3O_4.[34,35] All the other observed diffraction peaks are consistent with the standard card PDF # 80-1098 K-birnessite MnO_2,[34] suggesting that the K-birnessite MnO_2 can be successfully synthesized by hydrothermal reaction. Figure 1d shows the Raman spectrum of the material with feature peaks located at 190, 270, 398, 468, 500, 572 and 630 cm^{-1}, respectively [36,37]. Among them, the feature peak located at 630 cm^{-1} is resulted from the symmetric stretching vibration of v_2 (Mn-O) in the MnO_6 octahedron. The peak located at 572 cm^{-1} can be attributed to the stretching vibration of v_3 (Mn-O) the plane in the [MnO_6] sheet. According to previous reports,[38,39] the characteristic peak of 570~585 cm^{-1} is particularly intense in layered birnessite. Therefore, the strong feature peak located at 572 cm^{-1} suggests the layered structure of the K-birnessite MnO_2. Figure 1e shows the XPS results of Mn, O and K element states. The binding energies of Mn $2p_{1/2}$ and Mn $2p_{3/2}$ are 653.8 eV and 642.1 eV, respectively. And the energy difference between the two Mn 2P of 11.7 eV proves that K-birnessite MnO_2 is of high purity and successful synthesis. Mn $2p_{3/2}$ can be subdivided into three peaks that are Mn^{4+} (~ 642.9 eV), Mn^{3+} (~ 641.89 eV) and Mn^{2+} (~ 640.7 eV).[40,41] The existence of multiple oxidation states of Mn implies that the layered K-birnessite MnO_2 contains oxygen vacancies, which is confirmed in the high-resolution XPS spectrum of O 1s. The O 1s peak can be divided into three peaks with binding energies of ~ 532.2 eV, ~ 531.1 eV, and ~ 529.4 eV, respectively. Among them, the peak at 532.2 eV is the binding energy of H-O-H, corresponding to water molecules chemisorbed and physically adsorbed on the surface. The peak is found at 531.1 eV of the binding energy corresponded to oxygen vacancies, suggesting the oxygen defects formed during the synthesis of the layered K-birnessite MnO_2. The peak is evident at 529.4 eV originated from the binding

energy of Mn-O, suggesting the formation of K-birnessite MnO_2.[42,43] For K 2p, there are two spin sub-peaks including K $2p_{1/2}$ (~ 295.2 eV) and K $2p_{3/2}$ (~ 292.4 eV). The difference in the binding energy between the two sub-peaks is ~ 2.8 eV, which is consistent with previous reports.[40] The two sub-peaks can be fitted to K^+ and K^0, respectively.[44] All aforementioned characterizations demonstrate the successful synthesis of layered K-birnessite MnO_2 by the hydrothermal method.

In order to present the device from the 2D layers, the synthesized sample was transferred onto the Si/SiO_2 substrate to achieve individual K-birnessite MnO_2 nanosheet using scotch-tape by micromechanical exfoliation method. Thus, a series of characterizations have been carried out for the individual nanosheet. Figure 2a shows AFM image of the layered K-birnessite MnO_2 nanosheet after being transferred onto the Si/SiO_2 substrate. The top left illustration shows the optical image of the nanosheets, indicating that the prepared K-birnessite MnO_2 samples can be exfoliated into individual nanosheet. The AFM profile in the lower left illustration shows the exfoliated triangle thickness of ~ 25 nm.[45] Figure 2b shows bright-field TEM image of the K-birnessite MnO_2 nanosheet. The high-resolution TEM (HR-TEM) image shown at the upper right corner corresponds to the circled part in the main panel of Figure 2b. The lattice space is 2.53 Å, corresponding to (200) plane,[34,46] which is consistent with the data (~ 2.5292 Å) confirmed by the diffraction peak of (200) in the XRD pattern (Figure 1c). The Raman spectrum of the individual K-birnessite MnO_2 nanosheet (Figure 2c) shows six characteristic peaks in total at ~ 277, 401, 468, 504, 574 and 640 cm^{-1}, respectively.[37] The peak located at ~ 520 cm^{-1} is typically originated from silicon wafer. The six feature peaks are consistent with the prepared bulk K-birnessite MnO_2 samples, indicating that the individual nanosheet has been successfully transferred onto the substrate. Figure 2d shows PL spectrum of the K-birnessite MnO_2 nanosheet. The emission

peak sites at ~ 665 nm, suggesting the band gap energy of ~ 1.86 eV.[47] All the characterizations of the individual nanosheets suggest that the K-birnessite MnO_2 sample prepared by hydrothermal method can be mechanically exfoliated and transferred onto target substrates for the following device fabrication.

Then the RS device was prepared with lateral structure by using Ag as the two terminal electrodes through photolithography technique, as shown in Figure 3a of the device schematics. Figure 3b shows an optical image of the device with planar structure of Ag/ MnO_2/Ag on Si/SiO_2 substrate. The fabricated RS device with the channel length of ~ 4 μm based on the 2D nanosheet with the thickness of ~ 23 nm. Figure 3c shows the typical current–voltage (*I–V*) characteristics of the individual K-birnessite MnO_2 nanosheets in linear scale. It is known that the RS behaviors really depend on the device's processing. As shown in the inset of Figure 3c, no obvious RS loop can be observed in the initial *I–V* curve with the maximum bias voltage of 3 V. After several cycles, the RS behaviors can be detected, suggesting the forming process. In the typical RS *I–V* curve, as shown in Figure 3d, the high-resistance state (HRS) is suddenly changed to the low-resistance state (LRS) at ~ 0.60 V in the device, which means the "SET" process. The LRS can be retained in the bias range from 3 to 0 V. Then, in the negative scanning of 0 V to – 3 V, the LRS is transferred to HRS at – 0.24 V, suggesting a "RESET" process. The HRS can be maintained until a positive voltage is applied. These results confirm that the fabricated device is non-volatile with the ON/OFF current ratio up to ~ 2×10^5. In the whole measurement, the I_{cc} of 1 mA was applied to avoid destroying the device. It should be noted that the prepared 2D layered nanosheets possess similar thickness in the range of 20 to 30 nm with the triangle size between a few and dozens of microns in our experiments. The fabricated RS device shows comparable RS properties based on the MnO_2 nanosheets. To further understand the RS behaviors, the inset of

Figure 3d shows the enlarged graph in the positive voltage part of the *I–V* curve in double logarithmic coordinate axis. The initial state of the device is a HRS, and the slope is ~ 0.3 when a low voltage is applied to the device in the HRS. As the applied voltage increases, the fitting slope increases to ~ 2.07. This observation can be understand by the typical space charge limited current (SCLC) mechanism.[48] For the LRS, the slope is ~ 1.14. suggesting the Ohmic contact behaviors, which are consistent with the conducting filament (CF) model.[49] In the K-birnessite MnO_2 nanosheets, there are a large number of oxygen vacancies according to the XPS characterization. The oxygen vacancies may migrate under the bias voltage and form the CFs, giving rise to the observed LRS. Then, a reverse voltage can induce the reverse migration of oxygen vacancies and then the breakdown of CFs, inducing the subsequent HRS.

Then, the retention and endurance properties of the memristors were characterized at room temperature. The resistances of both HRS and LRS are recorded by the pulse voltages with the magnitude of 0.2 V, the pulse duration of 500 ms and the pulse duration of 5 s. Figure 4a shows the retention characteristics of the memristor. At the initial stage, there are some fluctuations for the LRS. Then the LRS shows a gradual decrease as time elapsed. While, the HRS remains almost unchanged during the entire period of measurement. The memristor shows good retention behaviors with the ON/OFF ratio up to 10^4 during the retention time up to 3.5×10^4 s. Figure 4b shows the endurance characteristics of the memory device under pulse conditions. The device is tested under the repetitive pulses with duration of 500 ms and magnitude of 3 V for SET and – 3 V for RESET. The HRS and LRS can be maintained up to 800 cycles without overlap between them. There is little fluctuation in both LRS and HRS. However, a relatively high ON/OFF ratio close to 10^4 can be achieved. Thus, we successfully prepared a non-volatile memory based on

individual K-birnessite MnO_2 nanosheet with the good retention and endurance behaviors, which shows good reproducibility and reliability of the memristors for applications.

All aforementioned RS behaviors were measured with the I_{cc} of 1 mA. It is intriguing that the nonvolatile MS behaviors can be changed into the volatile TS behaviors by decreasing the I_{cc}. Figure 5a shows the TS behaviors with I_{cc} of 100 μA under the work voltages of ± 5 V in the scan sequence of 0 V → 5 V → 0 V → –5 V → 0 V. The SET and RESET processes occur at the same polarity voltages, at ~ 3 V (– 3 V) and ~ 0.40 V (– 0.35 V), respectively. For the scanning in the positive side, the initial HRS can be switched into the LRS at ~ 3 V, i.e., the SET process. While the LRS is not stable and reverted to the HRS at ~ 0.40 V, i.e., the RESET process. For the scanning in the negative side, the device exhibits nearly symmetric RS loop to that of the positive scanning, indicating that the device has bidirectional TS characteristics. Importantly, the current ON/OFF ratio still can reach up to nearly 10^5, which is favorable for the peripheral circuit to recognize the existence state of the device. Next, as shown in the Figure 5b, we continue to decrease the I_{cc} to 10 μA, the device shows similar TS behaviors to those of the 100 μA. Furthermore, the nonvolatile MS behaviors also can be reverted when the I_{cc} is increased to 1 mA. Thus, the I_{cc} can effectively tune the RS behaviors between MS and TS in the K-birnessite MnO_2 nanosheets.

Generally, there are two modes of RS including nonvolatile MS and volatile TS. Both the LRS and HRS can be retained after removing the bias voltage in the MS mode. On the other hand, the LRS will return to the HRS when the bias voltage is decreased to a threshold value in the TS mode.[50] The former MS shows promising applications in data storage and the recently developed multifunctional synaptic neurons, while the latter TS demonstrates potential applications in the suppression of crosstalk current in the crossbar array.[51] The controllable transformation between

TS and MS can generally be achieved in a single RS device when suitable external stimulation is applied.[51–53] Typically, the transition can be achieved by setting different I_{cc}. Thus, in electronic and optoelectronic applications, the device can work in both MS and TS modes and be used as a memory or a selector through tuning the compliance current levels. Such devices with multi-functions would be helpful for simplifying the integrated process and technology. In our experiments, a relatively high I_{cc} (1 mA) can trigger the non-volatile MS behaviors, while a relatively low I_{cc} ($\leq$ 100 μA) can generate volatile TS characteristics. When the device is at a relatively low I_{cc}, some weak conductive filaments (CFs) can be formed in the MnO_2 nanosheets, inducing the LRS. However, the generated CFs are unstable. And such CFs can be spontaneously dissolved due to Joule heat induced by the electric current, resulting the recovery of the HRS when the applied voltage is decreased to zero under the identical polarity. Thus, the rupture of the unstable CFs leads to the TS behaviors in the 2D layered K-birnessite MnO_2 nanosheets. For MS behaviors, the relatively high I_{cc} can contribute to the formation of the stable CFs, which cannot be damaged by the Joule heat generated by the electric current. Thus, the breakdown of the stable CFs needs reverse and large voltage, giving rise to the MS behaviors in K-birnessite MnO_2 nanosheets. Therefore, through setting different I_{cc}, reversible transition between nonvolatile MS and bidirectional TS can be experimentally achieved in K-birnessite MnO_2 nanosheets.

CONCLUSIONS

In summary, we prepared memristors based on single K-birnessite MnO_2 nanosheets with Ag electrodes. The device exhibits nonvolatile MS behaviors with high current ON/OFF ratio of ~ 2×10^5, long retention time up to 3.5×10^4 s, and good endurance of 800 cycles. It is intriguing that the nonvolatile MS behaviors can be changed into the volatile TS behaviors by decreasing the I_{cc}.

And more importantly, the nonvolatile MS behaviors can be reverted when the I_{cc} is increased to 1 mA. Thus, reversible transition between the nonvolatile MS and volatile TS can be achieved in the single layered K-birnessite MnO_2 nanosheets through tuning the external stimulations of the I_{cc}. A relatively high I_{cc} (1 mA) can trigger the non-volatile MS behaviors, while a relatively low I_{cc} ($\leq$ 100 μA) can generate volatile TS characteristics. The transformation from MS to TS can be ascribed to the spontaneous breakdown of weak CFs formed at low I_{cc}. This work would provide guidelines for complex RS types based on 2D oxide nanosheets and help one to understand the underlying physical mechanism of different RS types in the 2D platform.

AUTHOR INFORMATION

Corresponding Author

Wenjing Jie: College of Chemistry and Materials Science, Sichuan Normal University, Chengdu, 610066, China. Email: wenjing.jie@sicnu.edu.cn

Jianhua Hao: Department of Applied Physics, The Hong Kong Polytechnic University, Hung Hom, Kowloon, Hong Kong, China. Email: jh.hao@polyu.edu.hk

Notes

The authors declare no competing financial interest.

ACKNOWLEDGMENT

This work was supported by the grants from National Natural Science Foundation of China (No. 61804023, No. 61971108, and No. 61974097), the Open Foundation of State Key Laboratory of Electronic Thin Films and Integrated Devices (KFJJ201805), the Open Foundation of National

Engineering Research Center of Electromagnetic Radiation Control Materials (ZYGX2019K003-1), Sichuan Youth Science and Technology Foundation (19JCQN0106), Key R&D Program of Sichuan Province (No. 2018GZ0527) and Hong Kong RGC GRF (PolyU 153033/17P).

REFERENCES

(1) Stark, M. S.; Kuntz, K. L.; Martens, S. J.; Warren, S. C. Intercalation of Layered Materials from Bulk to 2D. *Adv. Mater.* **2019**, *31* (27), 1808213.
(2) Hong, X.; Tan, C.; Chen, J.; Xu, Z.; Zhang, H. Synthesis, Properties and Applications of One- and Two-Dimensional Gold Nanostructures. *Nano Res.* **2014**, *8* (1), 40–55.
(3) Xue, W.; Gao, S.; Shang, J.; Yi, X.; Liu, G.; Li, R. W. Recent Advances of Quantum Conductance in Memristors. *Adv. Electron. Mater.* **2019**, *5* (9), 1800854.
(4) Bertolazzi, S.; Bondavalli, P.; Roche, S.; San, T.; Choi, S. Y.; Colombo, L.; Bonaccorso, F.; Samorì, P. Nonvolatile Memories Based on Graphene and Related 2D Materials. *Adv. Mater.* **2019**, *31* (10), 1806663.
(5) Liu, N.; Zhou, S.; Gao, N.; Zhao, J. Tuning Schottky Barriers for Monolayer GaSe FETs by Exploiting A Weak Fermi Level Pinning Effect. *Phys. Chem. Chem. Phys.* **2018**, *20* (33), 21732–21738.
(6) Jie, W.; Yang, Z.; Bai, G.; Hao, J. Luminescence in 2D Materials and Van der Waals Heterostructures. *Adv. Opt. Mater*. 2018, *6* (10), 1701296.
(7) Jie, W.; Hao, J. Graphene-Based Hybrid Structures Combined with Functional Materials of Ferroelectrics and Semiconductors. *Nanoscale* 2014, *6* (12), 6346–6362.
(8) Yang, S.; Song, X.; Zhang, P.; Gao, L. Facile Synthesis of Nitrogen-Doped Graphene-Ultrathin MnO_2 Sheet Composites and Their Electrochemical Performances. *ACS Appl. Mater. Interfaces* **2013**, *5* (8), 3317–3322.
(9) Xiong, P.; Ma, R.; Sakai, N.; Bai, X.; Li, S.; Sasaki, T. Redox Active Cation Intercalation/Deintercalation in Two-Dimensional Layered MnO_2 Nanostructures for High-Rate Electrochemical Energy Storage. *ACS Appl. Mater. Interfaces* **2017**, *9* (7), 6282–6291.
(10) Ma, R.; Bando, Y.; Zhang, L.; Sasaki, T. Layered MnO_2 Nanobelts: Hydrothermal Synthesis and Electrochemical Measurements. *Adv. Mater.* **2004**, *16* (11), 918–922.
(11) Ching, S.; Petrovay, D. J.; Jorgensen, M. L.; Suib, S. L. Sol-Gel Synthesis of Layered Birnessite-Type Manganese Oxides. *Inorg. Chem.* **1997**, *36* (5), 883–890.
(12) Kanoh, H.; Tang, W.; Makita, Y.; Ooi, K. Electrochemical Intercalation of Alkali-Metal Ions into Birnessite-Type Manganese Oxide in Aqueous Solution. *Langmuir* **1997**, *13* (25), 6845–6849.
(13) Ammundsen, B.; Paulsen, J. Novel Lithium-Ion Cathode Materials Based on Layered Manganese Oxides. *Adv. Mater.* **2001**, *13* (12–13), 943–956.
(14) Ge, J.; Zhuo, L.; Yang, F.; Tang, B.; Wu, L.; Tung, C. One-Dimensional Hierarchical Layered K_xMnO_2 ($x < 0.3$) Nanoarchitectures: Synthesis, Characterization, and Their Magnetic Properties. *J. Phys. Chem. B* **2006**, *110* (36), 17854–17859.

(15) Zhou, G.; Sun, B.; Ren, Z.; Wang, L.; Xu, C.; Wu, B.; Li, P.; Yao, Y.; Duan, S. Resistive Switching Behaviors and Memory Logic Functions in Single MnO_x Nanorod Modulated by Moisture. *Chem. Commun.* **2019**, *55* (67), 9915–9918.
(16) Du, H.; Chen, J.; Tu, M.; Luo, S.; Li, S.; Yuan, S.; Gong, T.; Huang, W.; Jie, W.; Hao, J. Transition from Nonvolatile Bipolar Memory Switching to Bidirectional Threshold Switching in Layered MoO_3 Nanobelts. *J. Mater. Chem. C* **2019**, *7* (39), 12160–12169.
(17) Qian, K.; Tay, R. Y.; Nguyen, V. C.; Wang, J.; Cai, G.; Chen, T.; Teo, E. H. T.; Lee, P. S. Hexagonal Boron Nitride Thin Film for Flexible Resistive Memory Applications. *Adv. Funct. Mater.* **2016**, *26* (13), 2176–2184.
(18) Liu, S.; Lu, N.; Zhao, X.; Xu, H.; Banerjee, W.; Lv, H.; Long, S.; Li, Q.; Liu, Q.; Liu, M. Eliminating Negative-SET Behavior by Suppressing Nanofilament Overgrowth in Cation-Based Memory. *Adv. Mater.* **2016**, *28* (48), 10623–10629.
(19) Yao, J.; Lin, J.; Dai, Y.; Ruan, G.; Yan, Z.; Li, L.; Zhong, L.; Natelson, D.; Tour, J. M. Highly Transparent Nonvolatile Resistive Memory Devices from Silicon Oxide and Graphene. *Nat. Commun.* **2012**, *3* (1), 1038.
(20) Zhao, F.; Wang, L.; Zhao, Y.; Qu, L.; Dai, L. Graphene Oxide Nanoribbon Assembly toward Moisture-Powered Information Storage. *Adv. Mater.* **2017**, *29* (3), 1604972.
(21) Cheng, P.; Sun, K.; Hu, Y. H. Memristive Behavior and Ideal Memristor of 1T Phase MoS_2 Nanosheets. *Nano Lett.* **2016**, *16* (1), 572–576.
(22) Li, D.; Wu, B.; Zhu, X.; Wang, J.; Ryu, B.; Lu, W. D.; Lu, W.; Liang, X. MoS_2 Memristors Exhibiting Variable Switching Characteristics toward Biorealistic Synaptic Emulation. *ACS Nano* **2018**, *12* (9), 9240–9252.
(23) Sangwan, V. K.; Jariwala, D.; Kim, I. S.; Chen, K. S.; Marks, T. J.; Lauhon, L. J.; Hersam, M. C. Gate-Tunable Memristive Phenomena Mediated by Grain Boundaries in Single-Layer MoS_2. *Nat. Nanotechnol.* **2015**, *10* (5), 403–406.
(24) Sangwan, V. K.; Lee, H. S.; Bergeron, H.; Balla, I.; Beck, M. E.; Chen, K. S.; Hersam, M. C. Multi-Terminal Memtransistors from Polycrystalline Monolayer Molybdenum Disulfide. *Nature* **2018**, *554* (7693), 500–504.
(25) Yang, Y.; Du, H.; Xue, Q.; Wei, X.; Yang, Z.; Xu, C.; Lin, D.; Jie, W.; Hao, J. Three-Terminal Memtransistors Based on Two-Dimensional Layered Gallium Selenide Nanosheets for Potential Low-Power Electronics Applications. *Nano Energy* **2019**, *57*, 566–573.
(26) Cao, Y.; Tian, X.; Gu, J.; Liu, B.; Zhang, B.; Song, S.; Fan, F.; Chen, Y. Covalent Functionalization of Black Phosphorus with Conjugated Polymer for Information Storage. *Angew. Chemie Int. Ed.* **2018**, *57* (17), 4543–4548.
(27) Bessonov, A. A.; Kirikova, M. N.; Petukhov, D. I.; Allen, M.; Ryhänen, T.; Bailey, M. J. A. Layered Memristive and Memcapacitive Switches for Printable Electronics. *Nat. Mater.* **2015**, *14* (2), 199–204.
(28) Lu, K.; Hu, Z.; Xiang, Z.; Ma, J.; Song, B.; Zhang, J.; Ma, H. Cation Intercalation in Manganese Oxide Nanosheets: Effects on Lithium and Sodium Storage. *Angew. Chemie Int. Ed.* **2016**, *55* (35), 10448–10452.
(29) Zhai, W.; Wang, C.; Yu, P.; Wang, Y.; Mao, L. Single-Layer MnO_2 Nanosheets Suppressed Fluorescence of 7-Hydroxycoumarin: Mechanistic Study and Application for Sensitive Sensing of Ascorbic Acid in Vivo. *Anal. Chem.* **2014**, *86* (24), 12206–12213.

(30) Zhou, C.; Wang, J.; Liu, X.; Chen, F.; Di, Y.; Gao, S.; Shi, Q. Magnetic and Thermodynamic Properties of α, β, γ and δ-MnO_2. *New J. Chem.* **2018**, *42* (11), 8400–8407.
(31) Shen, X. F.; Ding, Y. S.; Liu, J.; Cai, J.; Laubernds, K.; Zerger, R. P.; Vasiliev, A.; Aindow, M.; Suib, S. L. Control of Nanometer-Scale Tunnel Sizes of Porous Manganese Oxide Octahedral Molecular Sieve Nanomaterials. *Adv. Mater.* **2005**, *17* (7), 805–809.
(32) Zhang, X.; Yu, P.; Zhang, H.; Zhang, D.; Sun, X.; Ma, Y. Rapid Hydrothermal Synthesis of Hierarchical Nanostructures Assembled from Ultrathin Birnessite-Type MnO_2 Nanosheets for Supercapacitor Applications. *Electrochim. Acta* **2013**, *89*, 523–529.
(33) Wang, D.; Wang, L.; Liang, G.; Li, H.; Liu, Z.; Tang, Z.; Liang, J.; Zhi, C. A Superior δ-MnO_2 Cathode and a Self-Healing Zn-δ-MnO_2 Battery. *ACS Nano* **2019**, *13* (9), 10643–10652.
(34) Liu, Z.; Ma, R.; Ebina, Y.; Takada, K.; Sasaki, T. Synthesis and Delamination of Layered Manganese Oxide Nanobelts. *Chem. Mater.* **2007**, *19* (26), 6504–6512.
(35) Sun, Y.; Wang, L.; Liu, Y.; Ren, Y. Birnessite-Type MnO_2 Nanosheets with Layered Structures under High Pressure: Elimination of Crystalline Stacking Faults and Oriented Laminar Assembly. *Small* **2015**, *11* (3), 300–305.
(36) Iyer, A.; Del-Pilar, J.; King'Ondu, C. K.; Kissel, E.; Garces, H. F.; Huang, H.; El-Sawy, A. M.; Dutta, P. K.; Suib., S. L. Water Oxidation Catalysis Using Amorphous Manganese Oxides, Octahedral Molecular Sieves (OMS-2), and Octahedral Layered (OL-1) Manganese Oxide Structures. *J. Phys. Chem. C* **2012**, *116* (10), 6474–6483.
(37) Julien, C.; Massot, M.; Baddour-Hadjean, R.; Franger, S.; Bach, S.; Pereira-Ramos, J. P. Raman Spectra of Birnessite Manganese Dioxides. *Solid State Ion* **2003**, *159* (3–4), 345–356.
(38) Xia, H.; Zhu, X.; Liu, J.; Liu, Q.; Lan, S.; Zhang, Q.; Liu, X.; Seo, J. K.; Chen, T.; Gu, L.; Meng, Y.S. A Monoclinic Polymorph of Sodium Birnessite for Ultrafast And Ultrastable Sodium Ion Storage. *Nat. Commun.* **2018**, *9* (1), 5100.
(39) Zhou, J.; Yu, L.; Sun, M.; Yang, S.; Ye, F.; He, J.; Hao, Z. Novel Synthesis of Birnessite-Type MnO_2 Nanostructure for Water Treatment and Electrochemical Capacitor. *Ind. Eng. Chem. Res.* **2013**, *52* (28), 9586–9593.
(40) Barai, H. R.; Banerjee, A. N.; Joo, S. W. Improved Electrochemical Properties of Highly Porous Amorphous Manganese Oxide Nanoparticles with Crystalline Edges for Superior Supercapacitors; *J. Ind. Eng. Chem*. **2017**, *56*, 212–224.
(41) Zhang, L.; Lian, J.; Wu, L.; Duan, Z.; Jiang, J.; Zhao, L. Synthesis of a Thin-Layer MnO_2 Nanosheet-Coated Fe_3O_4 Nanocomposite as a Magnetically Separable Photocatalyst. *Langmuir* **2014**, *30* (23), 7006–7013.
(42) Yang, Q.; Wang, D.; Wang, C.; Li, X.; Li, K.; Peng, Y.; Li, J. Facile Surface Improvement Method for $LaCoO_3$ for Toluene Oxidation. *Catal. Sci. Technol.* **2018**, *8* (12), 3166–3173.
(43) Zhao, Y.; Zhang, J.; Wu, W.; Guo, X.; Xiong, P.; Liu, H.; Wang, G. Cobalt-Doped MnO_2 Ultrathin Nanosheets with Abundant Oxygen Vacancies Supported on Functionalized Carbon Nanofibers for Efficient Oxygen Evolution. *Nano Energy* **2018**, *54*, 129–137.
(44) Li, S.; Kang, E. T.; Neoh, K. G.; Ma, Z. H.; Tan, K. L.; Huang, W. In Situ XPS Studies of Thermally Deposited Potassium on Poly(p-Phenylene Vinylene) and Its Ring-Substituted Derivatives. *Appl. Surf. Sci.* **2001**, *181* (3–4), 201–210.

(45) Zhao, X.; Fan, Z.; Xu, H.; Wang, Z.; Xu, J.; Ma, J.; Liu, Y. Reversible Alternation between Bipolar and Unipolar Resistive Switching in Ag/MoS_2/Au Structure for Multilevel Flexible Memory. *J. Mater. Chem. C* **2018**, *6* (27), 7195–7200.
(46) Wang, X.; Li, Y. Selected-Control Hydrothermal Synthesis of α- and β-MnO_2 Single Crystal Nanowires. *J. Am. Chem. Soc.* **2002**, *124* (12), 2880–2881.
(47) Lu, A.; Li, Y.; Ding, H.; Xu, X.; Li, Y.; Ren, G.; Liang, J.; Liu, Y.; Hong, H.; Chen, N.; Chu, S.; Liu, F.; Li, Y.; Wang, H.; Ding, C.; Wang, C.; Lai, Y.; Liu, J.; Dick, J.; Liu, K.; Hochella, M. F. Photoelectric Conversion on Earth's Surface Via Widespread Fe- And Mn-Mineral Coatings. *Proc. Natl. Acad. Sci.* **2019**, *116* (20), 9741–9746.
(48) Bai, N.; Xu, M.; Hu, C.; Ma, Y.; Wang, Q.; He, D.; Qi, J.; Li, Y. Resistive Switching Behaviors Mediated by Grain Boundaries in One Longitudinal Al/MoS_2&PVP/ITO Device. *Mater. Sci. Semicond. Process.* **2019**, *91*, 246–251.
(49) Jeon, Y.-R.; Abbas, Y.; Sokolov, A. S.; Kim, S.; Ku, B.; Choi, C. Study of in Situ Silver Migration in Amorphous Boron Nitride CBRAM Device. *ACS Appl. Mater. Interfaces* **2019**, *11* (26), 23329–23336.
(50) Sun, H.; Liu, Q.; Li, C.; Long, S.; Lv, H.; Bi, C.; Huo, Z.; Li, L.; Liu, M. Direct Observation of Conversion Between Threshold Switching and Memory Switching Induced by Conductive Filament Morphology. *Adv. Funct. Mater.* **2014**, *24* (36), 5679–5686.
(51) Wang, H.; Du, Y.; Li, Y.; Zhu, B.; Leow, W. R.; Li, Y.; Pan, J.; Wu, T.; Chen, X. Configurable Resistive Switching between Memory and Threshold Characteristics for Protein-Based Devices. *Adv. Funct. Mater.* **2015**, *25* (25), 3825–3831.
(52) Pan, C.; Ji, Y.; Xiao, N.; Hui, F.; Tang, K.; Guo, Y.; Xie, X.; Puglisi, F. M.; Larcher, L.; Miranda, E.; Jiang, L.; Shi, Y.; Valov, I.; McIntyre, P.C.; Waser, R.; Lanza, M. Coexistence of Grain-Boundaries-Assisted Bipolar and Threshold Resistive Switching in Multilayer Hexagonal Boron Nitride. *Adv. Funct. Mater.* **2017**, *27* (10), 1604811.
(53) Chang, S. H.; Lee, J. S.; Chae, S. C.; Lee, S. B.; Liu, C.; Kahng, B.; Kim, D. W.; Noh, T. W. Occurrence of Both Unipolar Memory and Threshold Resistance Switching in a NiO Film. *Phys. Rev. Lett.* **2009**, *102* (2), 026801.

Figures

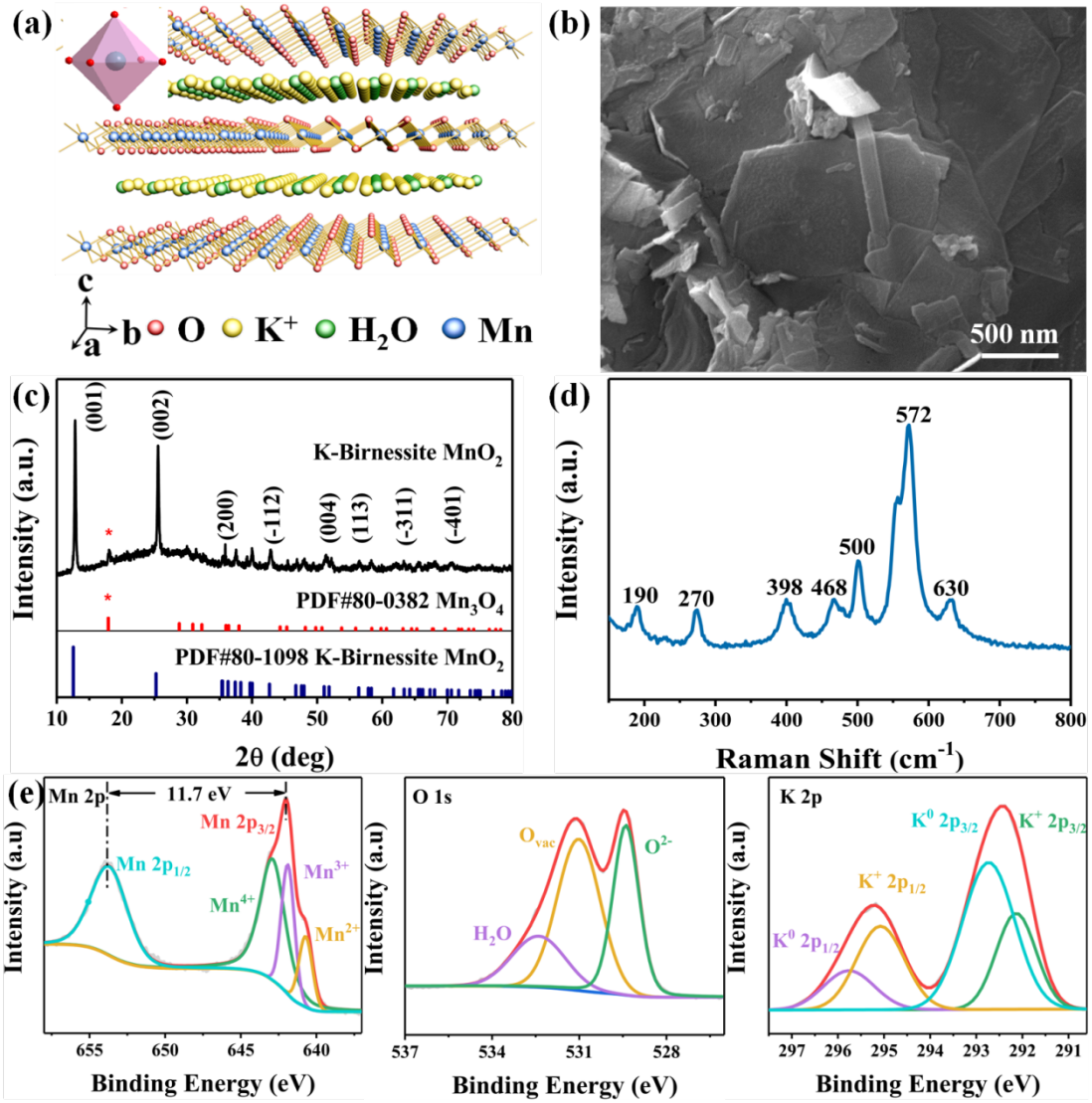

Figure 1. Characterization of bulk sample of layered K-birnessite MnO_2. (a) Schematic of atomic structure. Inset shows the MnO_6 octahedron. (b) Field emission scanning electron microscope image. (c) X-ray diffraction pattern. (d) Raman spectrum. (e) X-ray photoelectron spectroscope spectra of Mn, O and K element, respectively.

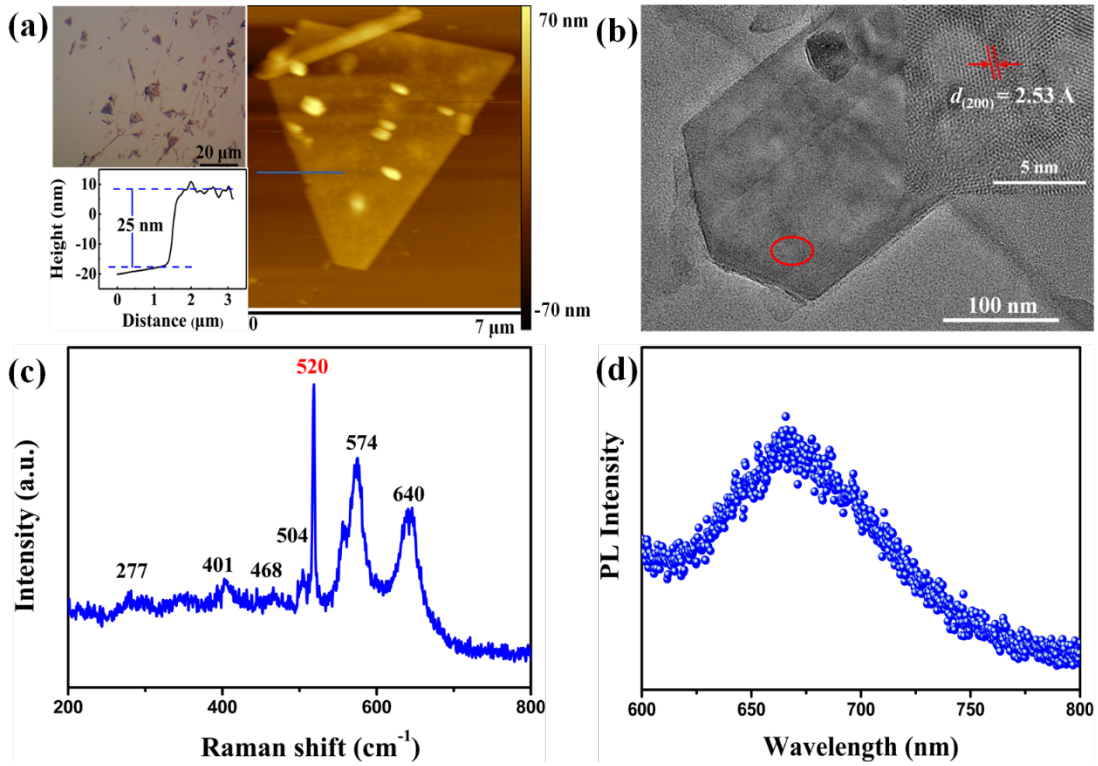

Figure 2. Characterization of the individual K-birnessite MnO_2 nanosheets. (a) The atomic force microscope image the layered K-birnessite MnO_2 nanosheets transferred onto the Si/SiO_2 substrate. Upper left illustration: optical image. Lower left illustration: height profile corresponding to the blue line in the AFM image. (b) The bright-field transmission electron microscope image of the nanosheet materials transferred onto the copper foil. The upper right corner shows the high-resolution TEM image. (c) Raman spectrum of the nanosheets transferred onto the Si/SiO_2 substrate. (d) Photoluminescence spectrum of the nanosheets transferred onto the Si/SiO_2 substrate.

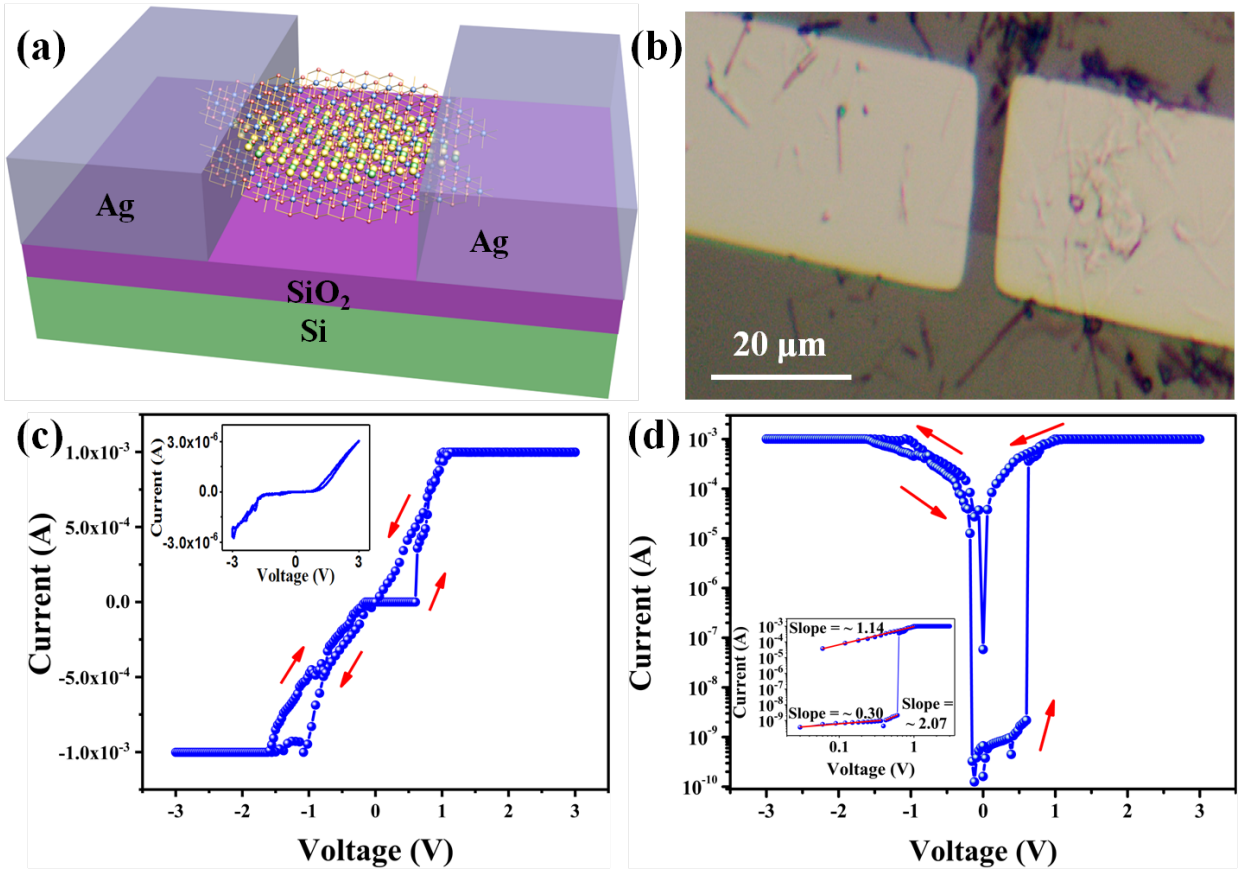

Figure 3. Measurements of the RS behaviors of the prepared of K-birnessite MnO_2 nanosheets. (a) Schematics and (b) optical image of the memristor based on individual K-birnessite MnO_2 nanosheet with Ag electrodes on Si/SiO_2 substrate. (c) Typical *I–V* curve of K-birnessite MnO_2 in linear scale. Inset: the initial *I–V* curve of the device before the forming process. (d) Typical *I–V* curve of K-birnessite MnO_2 with current in logarithmic scale. Inset is the re-plotted positive voltage part of the *I–V* curve in double logarithmic coordinate axis and linear fitting of the curve.

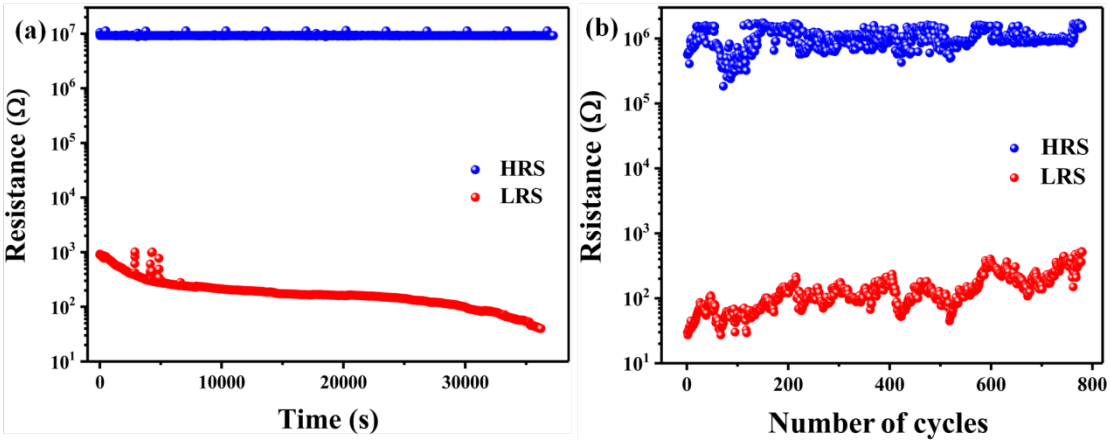

Figure 4. (a) Retention characteristics of memristor based on the individual K-birnessite MnO_2 nanosheets memory device with the compliance current of 1 mA at the voltage of 0.2 V. (b) Characterization of the cycle endurance for the memristor in the HRS and LRS.

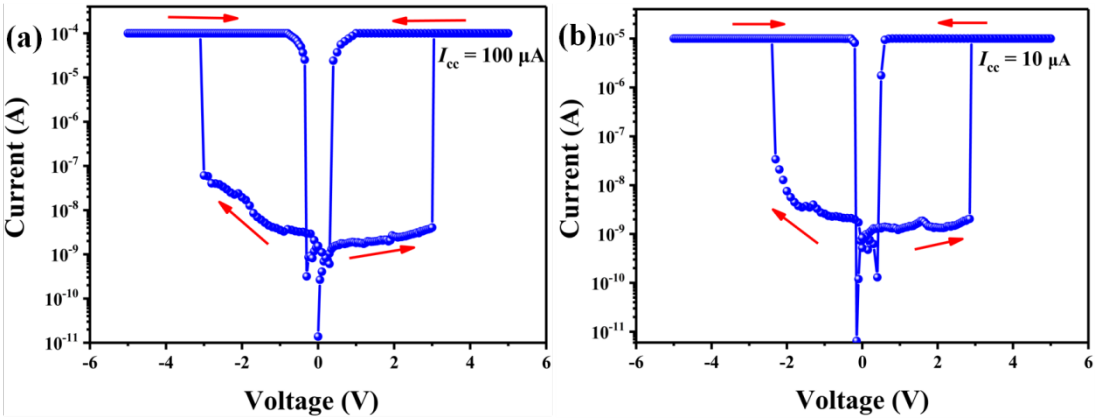

Figure 5. The TS behaviors of the prepared of K-birnessite MnO_2 nanosheets with different compliance current. (a) I_{cc} = 100 μA. (b) I_{cc} = 10 μA.

TOC

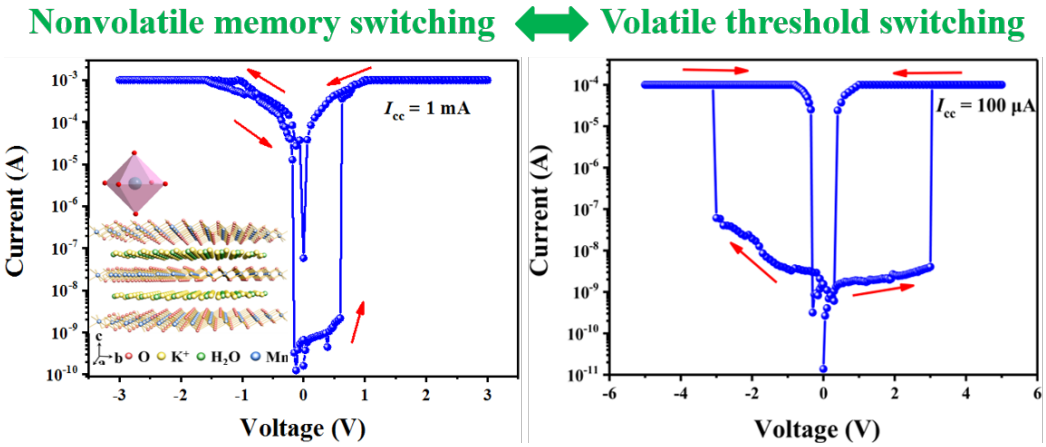
Nonvolatile memory switching
Volatile threshold switching
Current (A)
Voltage (V)
I_{cc} = 1 mA
O
K^+
H_2O
Mn
I_{cc} = 100 μA